Available on the CERN CDS information server **CMS PAS SUS-16-042**

CMS Physics Analysis Summary

Contact: cms-pag-conveners-susy@cern.ch 2017/03/28

Search for supersymmetry in events with one lepton and multiple jets in proton-proton collisions at $\sqrt{s} = 13$ TeV with 2016 data

The CMS Collaboration

Abstract

A search for supersymmetry is performed with proton-proton collision data recorded by the CMS experiment with a center-of-mass energy of 13 TeV and an integrated luminosity of 35.9 fb^{-1}. Data containing a single lepton are sorted into several exclusive search regions based on the number of jets and b-tagged jets, the scalar sum of the jet transverse momenta, and the scalar sum of the missing transverse momentum and the transverse momentum of the lepton. The observed number of events are consistent with the background expectation and the results are interpreted with two simplified supersymmetric models of gluino pair production. In the first model, each gluino decays via a three-body process to top quarks and a neutralino, which is associated with the observed missing transverse momentum in the event. Gluinos with masses up to 1.8 TeV are excluded for neutralino masses below 800 GeV. In the second model, each gluino decays via a three-body process to two light quarks and a chargino, which subsequently decays to a W boson and a neutralino. The mass of the chargino is taken to be midway between the gluino and neutralino masses. In this model, gluinos with masses below 1.9 TeV are excluded for neutralino masses below 300 GeV.

1 Introduction

Supersymmetry (SUSY) [1–8] remains as one of the most promising extensions of the standard model (SM) of particle physics. The addition of supersymmetric particles can lead to the cancellation of quadratically divergent loop corrections to the squared mass of the Higgs boson, while in SUSY models that conserve *R*-parity [9] the Lightest SUSY Particle (LSP) is stable and can be a viable dark matter candidate.

This Note presents an inclusive search for SUSY in the single-lepton channel with 13 TeV data recorded in 2016 by the CMS experiment at the CERN LHC and corresponding to an integrated luminosity of $36\,\text{fb}^{-1}$. The analysis is an update of a search performed in 2015 [10]. Similar searches were performed by the CMS and ATLAS experiments at lower center-of-mass energies, at 7 TeV [11–13], 8 TeV [14–16] and 13 TeV [17–19].

The results are interpreted within simplified models [20–23] of gluino pair production, in which the LSP is the lightest neutralino, $\widetilde{\chi}_1^0$, and the lepton is expected from the decay of a W boson that stems either from a top quark or a chargino ($\widetilde{\chi}_1^\pm$) decay. In the T1tttt model, shown in Fig. 1 (left), gluinos, denoted as $\widetilde{\text{g}}$, undergo three-body decays to $\text{t}\bar{\text{t}} + \widetilde{\chi}_1^0$. In the T5qqqqWW model, shown in Fig. 1 (right), the gluinos undergo three-body decays to a first- or second-generation quark-antiquark pair ($\text{q}\bar{\text{q}}$) and a $\widetilde{\chi}_1^\pm$. The chargino is taken to have a mass of $m_{\widetilde{\chi}_1^\pm} = 0.5(m_{\widetilde{\text{g}}} + m_{\widetilde{\chi}_1^0})$ and decays to a $\widetilde{\chi}_1^0$ and an W boson, which can be real or virtual, depending on the difference in mass between the $\widetilde{\chi}_1^\pm$ and the $\widetilde{\chi}_1^0$.

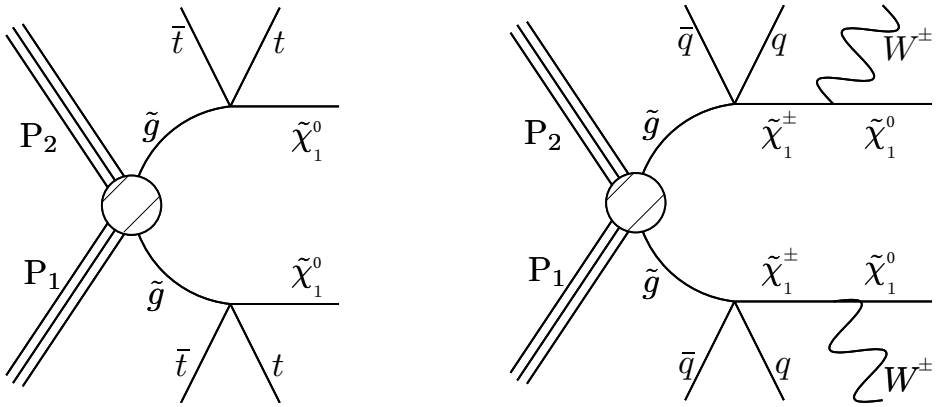

Figure 1: Diagrams showing the simplified models (left) T1tttt and (right) T5qqqqWW. Depending on the mass difference between the chargino ($\widetilde{\chi}_1^\pm$) and the neutralino ($\widetilde{\chi}_1^0$), the W boson can be virtual.

2 The CMS detector

The central feature of the CMS apparatus is a superconducting solenoid of 6 m internal diameter, providing a magnetic field of 3.8 T. A silicon pixel and strip tracker, a lead tungstate crystal electromagnetic calorimeter (ECAL), and a brass and scintillator hadron calorimeter (HCAL), each composed of a barrel and two endcap sections, reside within the solenoid volume. Forward calorimeters extend the pseudorapidity (η) [24] coverage provided by the barrel and endcap detectors. Muons are measured in the range $|\eta| < 2.4$, with detection planes made using three technologies: drift tubes, cathode strip chambers, and resistive plate chambers.

A more detailed description of the CMS detector, together with a definition of the coordinate system used and the relevant kinematic variables, can be found in Ref. [24].

3 Event reconstruction and simulation

The particle-flow event algorithm [25, 26] reconstructs and identifies each individual particle with an optimized combination of information from the various elements of the CMS detector. The energy of electrons is determined from a combination of the electron momentum at the primary interaction vertex as determined by the tracker, the energy of the corresponding ECAL cluster, and the energy sum of all bremsstrahlung photons spatially compatible with originating from the electron track [27]. The energy of muons is obtained from the curvature of the corresponding track [28].

The degree of isolation of a lepton from other particles provides a strong indication of whether it was produced in a hadronic jet, such as a jet resulting from the fragmentation of a b quark, or in the leptonic decay of a W boson, which can be produced promptly or in the decays of heavy particles like the top quark. Lepton isolation is quantified by performing a scalar sum of the transverse momenta (p_T) of all particles within a cone around the lepton momentum vector, excluding the contribution of the lepton itself. To maintain high efficiency for signal events, which typically contain a large number of jets from the SUSY decay chains, a p_T-dependent cone radius, R, is used: $R = (0.2, 10\,\text{GeV}/p_T[\text{GeV}], 0.05)$ for $(p_T < 50\,\text{GeV}, 50\,\text{GeV} < p_T < 200\,\text{GeV}, p_T > 200\,\text{GeV})$. The isolation variable is defined as a relative quantity, I_{rel}, by dividing the scalar sum by the p_T^ℓ of the lepton. Muons and electrons are required to satisfy $I_{rel} < 0.2$ and $I_{rel} < 0.1$ respectively. Additional leptons used in the event veto described below are required to satisfy $I_{rel} < 0.4$. In the calculation of the isolation variable, an area-based correction is employed to remove the contribution of particles from additional proton-proton collisions within the same or neighboring bunch crossings (pileup).

The energy of charged hadrons is determined from a combination of their momentum measured in the tracker and the matching ECAL and HCAL energy deposits, corrected for zero-suppression effects and for the response function of the calorimeters to hadronic showers. Finally, the energy of neutral hadrons is obtained from the corresponding corrected ECAL and HCAL energy.

Jets are clustered with the anti-k_T algorithm [29] with a distance parameter of 0.4 [30], as implemented in the FASTJET package [31]. The momentum of a jet, which is determined as the vectorial sum of all particle momenta in the jet, is found from simulation to be within 5 to 10% of the true momentum over the full p_T spectrum and detector acceptance. An offset correction is applied to jet energies to take into account the contribution from pileup [32]. Jet energy corrections are derived from simulation, and are confirmed with in-situ measurements of the energy balance in dijet and photon+jet events [33]. Additional selection criteria are applied to each event to remove spurious jet-like features originating from isolated noise patterns in certain HCAL regions.

To identify jets originating from b quarks, an inclusive combined secondary vertex tagger (CSVv2) [34, 35], which employs both secondary vertex and track-based information, is employed. The working point is chosen to result in a b-tagging efficiency and a light-flavor misidentification rate [36] of approximately 55–70%, depending on the jet p_T and η range, and 1.5%, respectively. Double counting of objects is avoided by not considering jets that lie within a cone of radius 0.4 around a selected lepton.

Monte Carlo simulation is used to estimate corrections to extrapolation factors that are extracted from data, and to determine some smaller backgrounds. The leading-order (LO) MADGRAPH5 [37] event generator, using the NNPDF3.0LO [38] parton distribution functions (PDFs), is used to simulate $t\bar{t}$+jets, W+jets, Z+jets, and multijet events. Single-top quark events in the t-

channel and the tW process are generated using the next-to-leading order (NLO) POWHEGv1.0 program [39–43]. The s-channel process, as well as $\mathrm{t\bar{t}W}$ and $\mathrm{t\bar{t}Z}$ production, are simulated using NLO MADGRAPH5_aMC@NLO [44]. The simulated background samples are normalized using the most accurate cross section calculations available [42–53], which generally correspond to NLO or next-to-NLO precision.

All signal events are generated with MADGRAPH5, with up to two partons in addition to the gluino pair. Both programs use the NNPDF3.0NLO [38] PDF. Gluino decays are based on a phase-space matrix element [54], with signal production cross sections computed at NLO with next-to-leading-logarithm (NLL) accuracy [55–59]

Several benchmark points, corresponding to different gluino and neutralino masses, are used for studying the kinematic properties of the signal processes and as illustration of the numbers of events expected from the SUSY processes. The points are denoted by the model name and the two key parameters, namely $m_{\tilde{g}}$ and $m_{\tilde{\chi}_1^0}$. As an example, the T1tttt(1.4,1.1) point corresponds to the T1tttt model with $m_{\tilde{g}} = 1.4\,\text{TeV}$ and $m_{\tilde{\chi}_1^0} = 1.1\,\text{TeV}$. A second point, T1tttt(1.9,0.1), is also used. Two benchmark points are also used for the T5qqqqWW model: T5qqqqWW(1.9,0.1) and T5qqqqWW(1.5,1.0). For both T5qqqqWW points, the mass of the intermediate chargino is taken to be 1.0 and 1.25 TeV respectively.

Showering and hadronization of all partons is performed using the PYTHIA 8.2 package [54]. Pileup is generated for a nominal distribution of the number of proton-proton interactions per bunch crossing, which is subsequently weighted to match the corresponding distribution observed in data. The detector response for all backgrounds is modelled using a detailed simulation based on the GEANT4 [60] package, while for the signal a fast simulation program [61] is used to reduce computation time. The fast simulation has been validated against the detailed GEANT4-based simulation for the variables relevant for this search, and efficiency corrections based on data are applied.

4 Trigger and event selection

The main trigger suite for this analysis is based on triggers containing a loosely isolated single lepton, electron or muon, with $p_{\mathrm{T}} > 15\,\text{GeV}$ and an online reconstructed H_{T}, the scalar sum of the jet p_{T}, of 350 GeV, raised to 400 GeV in later run periods. In order to maximise the overall efficiency, additional trigger paths have been added, requiring missing transverse momentum of 100, 110, or 120 GeV, depending on the run period, as well as requiring single leptons. The latter contain a threshold of 27(24) GeV for isolated electrons(muons), and higher thresholds for leptons without isolation requirement: 105 GeV (and in later run periods 115 GeV) for electrons and 50 GeV for muons. The trigger efficiency has been measured in both, control samples with single lepton triggers as reference and hadronic control samples using triggers with either an online reconstructed H_{T} requirement or a single jet as reference. After the offline event selection requirements applied in the current analysis, an overall trigger efficiency of 98(100)$\pm$1% is observed for the electron (muon) channel.

A minimum p_{T} of 25 GeV is required for electron or muon candidates. Events with additional electrons or muons with $p_{\mathrm{T}} > 10\,\text{GeV}$, satisfying looser selection criteria, referred to as "veto" leptons, are rejected. The main background in the signal region arises from $\mathrm{t\bar{t}}$+jets events where both W bosons decay leptonically and one lepton does not fulfill the quality criteria for veto leptons.

In an extension of the 2015 analysis, and in order to suppress this dileptonic $\mathrm{t\bar{t}}$+jets background,

events containing an isolated high-p_T charged track are rejected. The high-p_T track might be caused by hadronic decays of τ leptons or low-quality muons or electrons. The relative isolation of such tracks within a cone of $R = 0.3$ around the track candidate is required to be smaller than 0.1 (0.2) for hadronic (leptonic) particle flow candidates. For events containing such isolated track candidates, the M_{T2} variable [62] is used:

$$M_{T2}(\vec{\ell}, \vec{t}, \vec{p}_T^{\,miss}) = \min_{\vec{p}_{T1}+\vec{p}_{T2}=\vec{p}_T^{\,miss}} \max\left\{ M_T(\vec{\ell}, \vec{p}_{T1}), M_T(\vec{t}, \vec{p}_{T2}) \right\}, \quad (1)$$

where $\vec{t}$ and $\vec{\ell}$ are the momenta of the isolated track and the selected lepton respectively, $\vec{p}_T^{\,miss}$ is the missing transverse momentum, which is defined as the negative vector sum of the transverse momenta of all reconstructed particles in the event, and M_T is the transverse mass. The minimization runs over all possible splittings of the missing transverse momentum with the assumption of two lost massless particles, as in dileptonic $t\bar{t}$ decays that contain two neutrinos. The isolated track with the highest p_T and opposite charge with respect to the selected lepton is chosen. Events containing a hadronic (leptonic) isolated track with M_{T2} below $60(80)$ GeV are rejected. This rejects approximately 40% of dileptonic $t\bar{t}$+jets events, while only about 8–15% of the events from the different benchmark models are rejected in the signal regions given below.

Jets are required to have $p_T > 30$ GeV and $|\eta| < 2.4$. All search regions are required to contain at least five jets, while the two highest-p_T jets must satisfy $p_T > 80$ GeV. Different search regions, depending on the number of b-tagged jets, are identified. Regions with zero b-tagged jets, called "zero-b", are mainly sensitive to the T5qqqqWW model, while search regions with at least one b-tagged jet, called "multi-b", are sensitive to the T1tttt model. For the latter, the requirement on the number of jets is increased to six, since the presence of four top quarks results in an increased jet multiplicity in signal events.

The event selection criteria are completed with requirements on L_T, which is defined as the sum of p_T^{ℓ} and the magnitude of $\vec{p}_T^{\,miss}$, E_T^{miss}. A minimum L_T of 250 GeV is required, such that the analysis is sensitive not only to signals with high E_T^{miss}, but also to signals with small E_T^{miss} and higher lepton p_T. Due to trigger requirements and since a large hadronic activity is expected for the investigated SUSY models, H_T is required to be above 500 GeV.

After these selections, the main backgrounds arise from W+jets events with the W boson decaying leptonically, and $t\bar{t}$+jets events in which one of the W bosons from the top quarks decays to a charged lepton and a neutrino, and the other W boson decays hadronically. Both backgrounds are suppressed by requiring a large azimuthal angle $\Delta\Phi$ between the lepton and the presumed W boson. The transverse momentum of the leptonically decaying W boson is estimated as the vectorial sum of the lepton momentum, $\vec{p}_T^{\,\ell}$, and the transverse momentum vector, $\vec{p}_T^{\,miss}$. In background events from W+jets and $t\bar{t}$+jets with a single W-boson leptonic decay, the $\Delta\Phi$ distribution falls sharply and has a maximum value given by the mass and transverse momentum of the W boson. In the SUSY models investigated here, $\vec{p}_T^{\,miss}$ typically receives a large contribution from the two neutralino LSPs. As a consequence, large values of $\Delta\Phi$ are possible and the resulting $\Delta\Phi$ distribution in signal events is roughly uniform. The $\Delta\Phi$ variable is thus used to identify the search region (SR) as events with large $\Delta\Phi$ while events with small $\Delta\Phi$ constitute the control region (CR), which is used to estimate the SM background in the SR. The magnitude of the angle between the W boson and the lepton is inversely proportional to the W boson momentum. Therefore, the $\Delta\Phi$ threshold used in the definition of the signal region varies as a function of L_T, which is a measure of the W boson p_T, in the range 0.5 and 1. Exclusive search regions are defined by the number of jets (n_{jet}), the number of b-tagged jets (n_b),

H_T, and L_T.

The search is carried out in events with $\geq 6(5)$ jets in the multi-b (zero-b) analysis. For the estimation of the background in the SR, the CR of the same sample is used, along with a transfer factor that relates the numbers of events in the SR and CR. This transfer factor, which is the ratio of the number of background events in the SR and CR, is obtained from another sample which consists of events with a lower number of jets and is therefore depleted in signal.

The number of search bins has been updated with respect to the 2015 analysis: 39 search bins are used for the multi-b analysis and 28 search bins for the zero-b analysis. The definitions of the signal bins, along with the $\Delta\Phi$ values selected for the SR, are presented in Table 5 in the Appendix.

5 Background estimation

The method for estimating the background from SM processes is the same as the one presented in detail in Ref. [10]. For completeness, a summary is included here.

The dominant background in the SR, arising from semileptonic $\mathrm{t\bar{t}}$+jets and leptonic W+jets decays, is determined from the events in the CR, i.e. at low $\Delta\Phi$, and a transfer factor, R_{CS}, that relates the events expected in the CR to those in the SR. The transfer factor is measured using data in events with a lower number of jets, n_{jet}, where the contribution from the signal is negligible. Potential residual differences of the transfer factors in the low- and high-n_{jet} regions are determined through simulation. A correction factor, denoted by κ, is determined for each search bin. An overall correction factor is applied for the $n_b \geq 2$ search bins with the same H_T and L_T, since these factors are found to be essentially independent of n_b.

The regions with one b tag and four or five jets, consist of approximately 80% $\mathrm{t\bar{t}}$+jets and 15–20% W+jets and single top quark events. In all other multi-b regions the $\mathrm{t\bar{t}}$ background is dominant. Therefore, only one transfer factor is calculated in the multi-b analysis for each L_T, H_T and n_b range in the region with four or five jets, and applied for the multi-b in the regions with $n_{jet} \in [6-8]$ or $n_{jet} \geq 9$.

In the zero-b bins, the contributions from W+jets and $\mathrm{t\bar{t}}$+jets are roughly equal, and two extrapolation factors are determined in different sidebands for the two backgrounds for each of the search bins in n_{jet}, H_T and L_T. For the $\mathrm{t\bar{t}}$+jets estimate, these requirements are $n_{jet} \in [4,5]$ and $n_b \geq 1$, while the W+jets sideband is defined as $n_{jet} \in [3,4]$ and $n_b = 0$. For the latter, a lower jet multiplicity is chosen in order to limit the contamination from $\mathrm{t\bar{t}}$+jets events. The relative contribution of the two components is determined by a fit of the n_b multiplicity distribution in the CR of the high n_{jet} regions, using templates obtained from simulation. Additional backgrounds are found to be small and are taken from simulation.

About 10–15% of the SM background events in the CR are expected to be multijet events (denoted in the following as QCD), and arise mainly from jets misidentified as electrons or from photon conversions in the tracker. This background is estimated from data, using 'antiselected' events in which the electrons fail the criteria for selected electrons but satisfy looser identification and isolation requirements. These events are scaled by the ratio of jets and photons that pass the tight electron identification requirements to the number of antiselected electron candidates in a multijet-enriched control sample that consists of no b-tagged jets and three or four other jets. Since the multijet background is negligible in the SR, it is subtracted from the number of background events in the CR when calculating the transfer factor R_{CS}^{data} to extrapolate from CR (low-$\Delta\Phi$) to SR (high-$\Delta\Phi$). The usage of the various (n_{jet}, n_b) regions employed in the

analysis is illustrated in Table 1.

Table 1: Overview of the definitions of sideband and mainband regions. For the multijet (QCD) fit the electron (e) sample is used, while for the determination (det.) of $R_{CS}(W^{\pm})$ the muon (μ) sample is used. Empty cells are not used in the analysis.

<table>
<tr><td>Analysis</td><td colspan="2">Multi-b analysis</td><td colspan="2">Zero-b analysis</td></tr>
<tr><td></td><td>$n_b = 0$</td><td>$n_b \geq 1$</td><td>$n_b = 0$</td><td>$n_b \geq 1$</td></tr>
<tr><td>$n_{jet} = 3$</td><td rowspan="2">QCD bkg. fit (e sample)</td><td></td><td rowspan="2">$R_{CS}(W^{\pm})$ det. (μ sample), QCD bkg. fit (e sample)</td><td></td></tr>
<tr><td>$n_{jet} = 4$</td><td rowspan="2">R_{CS} det.</td><td rowspan="3">$R_{CS}(t\bar{t}$+jets) det.</td></tr>
<tr><td>$n_{jet} = 5$</td><td></td><td rowspan="2">search bins</td></tr>
<tr><td>$n_{jet} \geq 6$</td><td></td><td>search bins</td><td></td></tr>
</table>

6 Systematic uncertainties

Two categories of systematic uncertainties are identified: those that affect the estimates of the background from SM processes, and those that affect the expected signal yields.

The main systematic uncertainty on the background estimate arises from the extrapolation of R_{CS} from the low n_{jet} region, where it is measured, to the regions of higher n_{jet} where it is applied. The modeling of jets from initial-state radiation (ISR) is derived from data in a control region populated mainly by dileptonic $t\bar{t}$+jets events. This region is defined by two opposite-sign leptons (electrons or muons), excluding same-flavor leptons within a window of $\pm 10\,\text{GeV}$ around the Z-boson mass, and exactly two b-tagged jets, such that any other remaining jet is interpreted as an ISR jet. In simulation, all jets that cannot be matched to daughter particles from the hard interaction are treated as ISR jets. The difference between the numbers of ISR jets observed and simulated is then used to reweight simulated $t\bar{t}$+jets events in all analysis selections. The reweighting factors vary between 0.92 and 0.51 for N_J^{ISR} between 1 and 6. We take one half of the deviation from unity as the systematic uncertainty on these reweighting factors.

The ratio of the semileptonic to dileptonic $t\bar{t}$+jets final states differs in the CR and SR, with the fraction of dileptonic $t\bar{t}$+jets events being higher in the SR. It is important to have a good description of this ratio as a function of n_{jet} in the simulation, since the differences in the transfer factors between the low-n_{jet} and high-n_{jet} events, i.e. the κ factors, are determined in simulation. This is tested in a dilepton control sample, similar to the selection described in the previous paragraph, but split into a zero-b and multi-b category. To study the behavior of the dileptonic events that remain in the single-lepton selection because of the loss of the second lepton, one of the two leptons is removed from the event. Since these "lost leptons" arise principally from $\tau \to \text{hadrons} + \nu$ decays, and to account for the missing energy due to the neutrino from the τ decay, the lepton removed is replaced by a jet with 2/3 of the p_T of the original lepton and the L_T, $\Delta\Phi$, and H_T values are recalculated for the resulting "single-lepton" event. In order to maximize the number of events in the dileptonic $t\bar{t}$+jets control sample, no $\Delta\Phi$ requirement is applied, and all events are used twice, with each reconstructed lepton being considered as the lost lepton. The jet multiplicity for the data sample resulting from the single-lepton baseline selection (excluding the SRs) is compared with the corresponding simulated event sample, and the dilepton CRs in data are compared with the corresponding simulated event sample, forming a double-ratio. The remaining differences in the double-ratio are corrected for in the calculation of κ factors and propagated as systematic uncertainty.

Uncertainties in the background estimate, that also affect the signals yields, arise from un-

certainties in the jet energy scale (JES) [30], in the efficiencies and misidentification rate for b-tagging [35] and in the efficiency of lepton reconstruction and identification. In each case, the systematic uncertainty in the background is estimated by varying the corresponding correction factors within their uncertainty. In the case of the JES, the H_{T} and $E_{\mathrm{T}}^{\mathrm{miss}}$ of the event are recalculated following the variation of the JES correction factors. The additional uncertainty arising from pileup is estimated by varying the inelastic cross section within a 5% uncertainty [63].

The W+jets and $\mathrm{t\bar{t}}$+jets cross sections are varied by 30% [64] to account for possible biases in the estimation of the background composition in terms of W+jets *vs.* $\mathrm{t\bar{t}}$+jets events, which would lead to a slight change in the κ value. These changes have only a small impact on the zero-b analysis, where the relative fraction of the two processes is determined from a fit. In the multi-b analysis, the variation results in differences in the κ values which are propagated to the background estimate.

The polarization of W bosons is varied by reweighting events by the factor $w(\cos\theta^*) = 1 + \alpha(1 - \cos\theta^*)^2$, where θ^* is the angle between the charged lepton and W boson in the W boson rest frame. For W+jets events, $\alpha = 0.1$ is used, guided by the measurements and theoretical uncertainty [65–68]. For $\mathrm{t\bar{t}}$+jets events, $\alpha = 0.05$ is used.For W+jets events, where the initial state can have different polarizations for $\mathrm{W^+}$ and $\mathrm{W^-}$ bosons, the uncertainty is determined as the larger change in κ resulting from reweighting only the $\mathrm{W^+}$ bosons in the sample, and from reweighting all W bosons. The $\mathrm{t\bar{t}V}$ cross section is varied by 100%. The systematic uncertainty in the multijet estimation depends on n_{jet} and n_{b}, and ranges from 25% to 100%.

For the zero-b analysis, an additional systematic uncertainty is applied, based on linear fits of R_{CS} as a function of n_{jet}, and a 50% cross section uncertainty is used for all backgrounds other than W+jets, $\mathrm{t\bar{t}}$+jets, $\mathrm{t\bar{t}V}$, and multijets.

For the signal, an uncertainty in initial-state radiation (ISR) is applied using the approach described previously for the reweighting of the distribution of ISR jets in $\mathrm{t\bar{t}}$. Half of the correction is used as an estimate of the uncertainty and propagated towards the signal acceptance. The factorization and renormalization scales are changed by a factor of 0.5 and 2.

Finally, the luminosity is measured with the pixel cluster counting method, and the absolute luminosity scale calibration is obtained using Van der Meer scans and results in an uncertainty of 2.6% [69].

The impact of the systematic uncertainties in the total background estimate for the multi-b and zero-b analyses are summarized in Table 2. While the systematic uncertainty is determined for each signal point, typical values of the uncertainties for most signals are summarized for illustration in Table 3.

7 Results and interpretation

The backgrounds for all SRs are determined, as described previously, in different regions of lower jet or b-jet multiplicities. The result of the background estimates and the data observed are shown in Fig. 2 for the multi-b events. In this figure, the outline of the filled histogram represents the total estimated number of background events. For illustration, the relative amount of $\mathrm{t\bar{t}}$+jets, W+jets, and of other backgrounds is shown as well, based on the fractions estimated in simulation.

Figure 3 shows the estimates and data observed for the zero-b events. Here, the filled histogram represents the estimates from data for $\mathrm{t\bar{t}}$+jets and W+jets events and the remaining

Table 2: Summary of systematic uncertainties in the total background estimates for the multi-b and for the zero-b analyses.

Source	Uncertainty for multi-b [%]	Uncertainty for zero-b [%]
Dilepton control sample	0.9–7.0	0.3–18
JES	0.3–18	0.7–26
Tagging of b-jets	0.1–3.0	0.7–3.0
σ(W+jets)	0.3–9.3	0.3–10
$\sigma(\mathrm{t\bar{t}})$	0.1–7.5	0.7–13
$\sigma(\mathrm{t\bar{t}V})$	0.2–20	0.1–3.8
W polarization	0.1–3.3	0.7–13.8
nISR reweighting	0.5–7.0	0.2–11
Pileup	0.4–7.1	0.1–19.6
Statistical uncertainty in MC events	5–30	5.2–35.9

Table 3: Summary of the systematic uncertainties and their average effect on the yields for the benchmark points defined in the text. The values, which are quite similar for the multi-b and the zero-b analyses, are usually larger for compressed scenarios, where the mass difference between the gluino and the lightest neutralino is small.

Source	Uncertainty [%]
Trigger	2
Pileup	10
Lepton efficiency	2
Isolated track veto	4
Luminosity	2.6
ISR	2–25
Tagging of b-jets (heavy flavors)	1–6
Tagging of b-jets (light flavors)	1–4
JES	3–40
Factorization/renormalization scale	1–3
$E_{\mathrm{T}}^{\mathrm{miss}}$	2–20

backgrounds, which include the multijet estimate determined from data and rare backgrounds determined from simulation.

To facilitate the reinterpretation of the results in terms of other theoretical models, a comparison of the background estimates and the observed number of events in a few aggregated signal regions is presented in Table 4. The results for all search bins, compared to two benchmark points, are given in the Appendix in the Tables 6 and 7 for the multi-b and zero-b analysis, respectively. The data agree with the expectations from the SM and no significant excess is observed.

The absence of any significant excess consistent with the SUSY signals considered in the analysis is used to set limits in the parameter space of the gluino and lightest neutralino masses. To set limits, separate likelihood functions, one for the multi-b analysis and one for the zero-b analysis, are constructed from the poisson probability functions for all four data regions, i.e. the CRs and SRs at both high and low jet multiplicities, to determine the background in the SR with high jet multiplicity, where the signal is expected. In addition, the κ values that correct any residual differences in the transfer factors, *Rcs*, between the low and high jet multiplicity regions, are included. As explained previously, the values of κ are obtained from simulation; their uncertainties are incorporated in the likelihood through log-normal constraints. The estimated

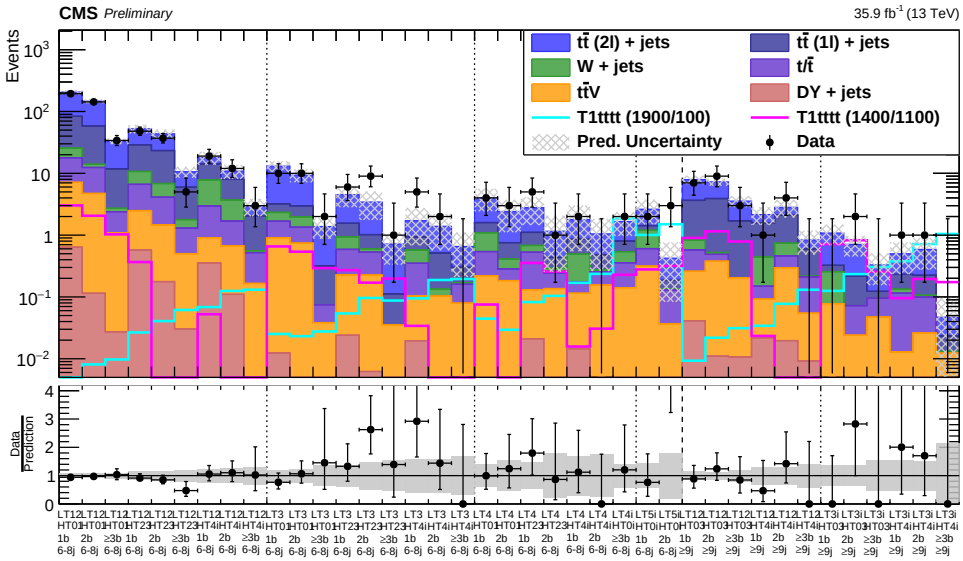

Figure 2: Multi-b search: comparison of the number of events observed in the data and the numbers expected from the estimated SM backgrounds in the 39 search bins defined in the text. Upper panel: the data are shown by black points with error bars, while the total SM background expected is shown as a grey line with a hatched region that represents the uncertainty. For illustration, the relative fraction of the different SM background contributions, as determined from simulation, is shown by the stacked, colored histograms, which are normalized so that their sum is equal to the background estimated using data control regions, as described in the text. The expected event yields for two T1tttt SUSY benchmark models are shown by open histograms. Lower panel: the ratio of the number of events observed in data to the number of events expected from the SM background, for each search bin. The error bars on the data points indicate the combined statistical and systematic uncertainty in the ratio. The grey hatched region indicates the uncertainty on the ratio that arises from the uncertainty on the background estimate.

Table 4: Number of expected background events and the measured number of events in the aggregated signal regions.

n_b	n_{jet}	L_T / GeV	H_T / GeV	Pred. background ($\pm$ stat)	Observed data
≥ 1	≥ 6	≥ 600	≥ 1000	11.18 ± 3.51	13
≥ 3	≥ 6	≥ 600	≥ 1000	0.84 ± 0.47	1
≥ 2	≥ 9	≥ 450	≥ 500	1.61 ± 0.41	3
≥ 2	≥ 9	≥ 450	≥ 1500	0.64 ± 0.32	1
≥ 3	≥ 9	≥ 250	≥ 500	4.58 ± 0.74	3
≥ 3	≥ 9	≥ 250	≥ 1500	0.81 ± 0.32	0
≥ 3	≥ 9	≥ 450	≥ 500	0.37 ± 0.16	0
≥ 3	≥ 9	≥ 450	≥ 1500	0.05 ± 0.05	0
0	≥ 5	≥ 650	≥ 750	18.37 ± 5.1	14
0	≥ 6	≥ 450	≥ 500	28.77 ± 6.8	37
0	≥ 6	≥ 650	≥ 1000	5.07 ± 1.8	4
0	≥ 7	≥ 450	≥ 500	9.73 ± 2.5	11
0	≥ 7	≥ 650	≥ 500	3.8 ± 1.2	4
0	≥ 8	≥ 250	≥ 1250	7.19 ± 1.9	8

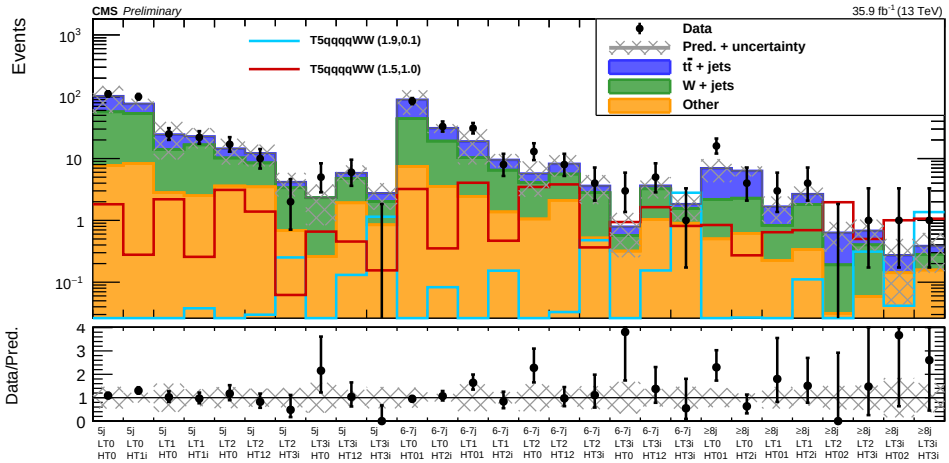

Figure 3: Zero-b search: comparison of the numbers of events observed in the data and the numbers expected from the estimated SM backgrounds in the 28 search bins defined in the text. Upper panel: the data are shown by black points with error bars, while the total SM background expected is shown as a grey line with a hatched region that represents the uncertainty. The filled, stacked histograms represent the predictions for $t\bar{t}$+jets, W+jets events, and the remaining backgrounds. The expected yields from two T5qqqqWW model points are shown as solid lines. lower panel: the ratio of the number of events observed in data to the number of events expected from the SM background, for each search bin. the error bars on the data points indicate the combined statistical and systematic uncertainty in the ratio. the grey hatched region indicates the uncertainty on the ratio that arises from the uncertainty on the background estimate.

contribution from multijet events in the CRs is also included. A possible signal contamination is taken into account by including signal terms in the likelihood for the low jet multiplicity regions as well as the control regions. For the zero-b analysis, the relative contributions from W+jets and $t\bar{t}$+jets events as determined in the fits to the n_b distribution in the CRs are treated as external measurements. The correlation between the W+jets and $t\bar{t}$+jets yields introduced by these fits is taken into account. A profile likelihood ratio is used as test statistic. The limits at

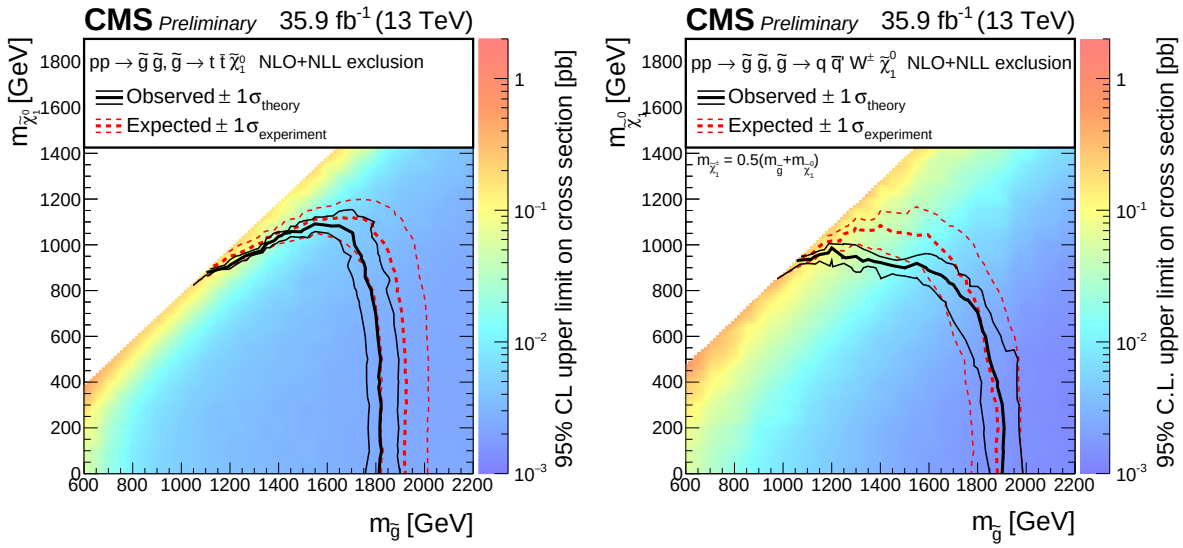

Figure 4: Cross section limits at a 95% CL for the (left) T1tttt and (right) T5qqqqWW models, as a function of the gluino and LSP masses. In T5qqqqWW, the pair-produced gluinos decay to a first- or second-generation quark-antiquark pair ($q\bar{q}$) and a chargino ($\widetilde{\chi}_1^{\pm}$) with its mass taken to be $m_{\widetilde{\chi}_1^{\pm}} = 0.5(m_{\widetilde{g}} + m_{\widetilde{\chi}_1^0})$. The solid black (dashed red) lines correspond to the observed (expected) mass limits, with the thicker lines representing the central values and the thinner lines representing the $\pm 1\sigma$ uncertainty bands related to the theoretical (experimental) uncertainties.

the 95% confidence level (CL) are calculated with the asymptotic formulae [70], using the CL_s criterion [71, 72].

The cross section limits obtained for the T1tttt model using the multi-b analysis, and for the T5qqqqWW model using the zero-b analysis, are shown in Fig. 4 as a function of $m_{\widetilde{g}}$ and $m_{\widetilde{\chi}_1^0}$, assuming branching fractions of 100%, as shown in Fig. 1. Using the $\widetilde{g}\widetilde{g}$ pair production cross section calculated at NLO within NLL accuracy, exclusion limits are set as a function of the $(m_{\widetilde{g}}, m_{\widetilde{\chi}_1^0})$ mass hypothesis.

8 Summary

A search for supersymmetry has been performed with 36 fb^{-1} of proton-proton collision data recorded by the CMS experiment at $\sqrt{s} = 13\,\text{TeV}$ in 2016. Several exclusive search bins, differing in the number of jets, the number of b-tagged jets, the scalar sum of all jet transverse momenta as well as the scalar sum of the missing transverse momentum and the transverse momentum of the lepton. The main background, which arises from W+jets and $\text{t}\bar{\text{t}}$+jets events, is reduced significantly by requiring a large azimuthal angle between the directions of the momenta of the lepton and of the reconstructed W boson, attributing all the $E_{\text{T}}^{\text{miss}}$ in the event to a neutrino from the leptonic decay of a W boson. The data observed are in agreement with the estimate of the standard model background, which is based on data samples and corrections based on simulation. The lack of any significant excess of events is interpreted in terms of limits on the parameters of two simplified models that describe gluino pair production.

For the T1tttt model, in which each gluino decays through an off-shell top squark to a $\text{t}\bar{\text{t}}$ pair and the lightest neutralino, gluino masses up to 1.8 TeV are excluded for neutralino masses below 800 GeV. Neutralino masses below 1.1 TeV can be excluded for a gluino mass up to 1.7 TeV.

The second simplified model, T5qqqqWW, also contains gluino pair production, with the gluinos

decaying to first- or second-generation squarks and a chargino, which subsequently decays to a W boson and the lightest neutralino. The chargino mass in this decay chain is taken to be $m_{\widetilde{\chi}_1^\pm} = 0.5(m_{\widetilde{g}} + m_{\widetilde{\chi}_1^0})$. In this model, gluino masses below 1.9 TeV are excluded for neutralino masses below 300 GeV. For a gluino mass of 1.2 TeV, neutralinos with masses up to 950 GeV can be excluded.

A Appendix

Table 5 contains the description of all signal regions, and Tables 6 and 7 contain the results for all search bins of the multi-b and zero-b analyses.

Table 5: Search regions and the corresponding minimum $\Delta\Phi$ requirements.

n_{jet}	n_{b}	L_{T} [GeV]	H_{T} [GeV]	$\Delta\Phi$ [rad]
[6,8]	=1; =2	[250,450]	[500,1000]	1.0
			[1000,1500]	
			> 1500	
		[450,600]	[500,1000]	0.75
			[1000,1500]	
			> 1500	
		[600,750]	[500,1000]	0.5
			[1000,1500]	
			> 1500	
		> 750	> 500	0.5
	≥ 3	[250,450]	[500,1000]	1.0
			[1000,1500]	
			> 1500	
		[450,600]	[500,1000]	0.75
			[1000,1500]	
			> 1500	
		> 600	> 500	0.5
≥ 9	=1; =2; ≥ 3	[250,450]	[500,1500]	1.0
			> 1500	
		> 450	[500,1500]	0.75
			> 1500	
5	0	[250,350]	[500,750]	1.0
			> 750	
		[350,450]	[500,750]	1.0
			> 750	
		[450,650]	[500,750]	0.75
			[750,1250]	
			> 1250	
		> 650	[500,750]	0.5
		[750,1250]		
			> 1250	
[6,7]	0	[250,350]	[500,1000]	1.0
			> 1000	
		[350,450]	[500,1000]	1.0
			> 1000	
		[450,650]	[500,750]	0.75
			[750,1250]	
			> 1250	
		> 650	[500,750]	0.5
			[750,1250]	
			> 1250	
≥ 8	0	[250,350]	[500,1000]	1.0
			> 1000	
		[350,450]	[500,1000]	1.0
			> 1000	
		[450,650]	[500,1250]	0.75
			> 1250	
		> 650	[500,1250]	0.5
			> 1250	

Table 6: Summary of the results in the multi-b search.

n_{jet}	n_{b}	L_{T} [GeV]	H_{T} [GeV]	Bin name	Expected signal T1tttt $m_{\tilde{g}}/m_{\tilde{\chi}^0}$ [TeV] (1.9,0.1)	(1.4,1.1)	Predicted background	Observed
[6, 8]	$= 1$	[250, 450]	[500, 1000]	NB1, LT12, HT01	< 0.01	3.02 ± 0.24	$206 \pm 12 \pm 9.4$	194
			[1000, 1500]	NB1, LT12, HT23	0.03 ± 0.01	0.37 ± 0.08	$53 \pm 7.4 \pm 3.6$	48
			≥ 1500	NB1, LT12, HT4i	0.07 ± 0.01	0.05 ± 0.03	$18 \pm 4.2 \pm 0.5$	19
		[450, 600]	[500, 1000]	NB1, LT3, HT01	0.03 ± 0.01	0.66 ± 0.11	$13 \pm 2.5 \pm 0.9$	10
			[1000, 1500]	NB1, LT3, HT23	0.05 ± 0.01	0.27 ± 0.07	$4.5 \pm 1.7 \pm 0.3$	6
			≥ 1500	NB1, LT3, HT4i	0.09 ± 0.01	0.03 ± 0.02	$1.7 \pm 1.0 \pm 0.3$	5
		[600, 750]	[500, 1000]	NB1, LT4, HT01	0.04 ± 0.01	0.08 ± 0.04	$4.0 \pm 1.5 \pm 0.5$	4
			[1000, 1500]	NB1, LT4, HT23	0.08 ± 0.01	0.35 ± 0.08	$2.8 \pm 1.3 \pm 0.2$	5
			≥ 1500	NB1, LT4, HT4i	0.17 ± 0.02	0.02 ± 0.02	$1.8 \pm 1.2 \pm 0.2$	2
		≥ 750	≥ 500	NB1, LT5i, HT0i	1.01 ± 0.04	0.28 ± 0.07	$2.6 \pm 1.1 \pm 0.2$	2
	$= 2$	[250, 450]	[500, 1000]	NB2, LT12, HT01	0.01 ± 0.01	2.06 ± 0.20	$147 \pm 9.4 \pm 5.5$	143
			[1000, 1500]	NB2, LT12, HT23	0.04 ± 0.01	< 0.01	$44 \pm 7.3 \pm 1.7$	37
			≥ 1500	NB2, LT12, HT4i	0.13 ± 0.01	< 0.01	$11 \pm 2.7 \pm 0.7$	12
		[450, 600]	[500, 1000]	NB2, LT3, HT01	0.02 ± 0.01	0.54 ± 0.10	$9.4 \pm 2.1 \pm 0.8$	10
			[1000, 1500]	NB2, LT3, HT23	0.10 ± 0.01	0.17 ± 0.06	$3.4 \pm 1.7 \pm 0.2$	9
			≥ 1500	NB2, LT3, HT4i	0.19 ± 0.02	< 0.01	$1.4 \pm 0.8 \pm 0.2$	2
		[600, 750]	[500, 1000]	NB2, LT4, HT01	0.03 ± 0.01	< 0.01	$2.4 \pm 1.2 \pm 0.4$	3
			[1000, 1500]	NB2, LT4, HT23	0.10 ± 0.01	0.26 ± 0.07	$1.2 \pm 0.9 \pm 0.2$	1
			≥ 1500	NB2, LT4, HT4i	0.24 ± 0.02	0.03 ± 0.02	$1.1 \pm 0.8 \pm 0.2$	0
		≥ 750	≥ 500	NB2, LT5i, HT0i	1.50 ± 0.05	0.32 ± 0.08	$0.42 \pm 0.34 \pm 0.05$	3
	≥ 3	[250, 450]	[500, 1000]	NB3i, LT12, HT01	0.01 ± 0.01	1.03 ± 0.14	$33 \pm 2.9 \pm 1.5$	34
			[1000, 1500]	NB3i, LT12, HT23	0.06 ± 0.01	< 0.01	$11 \pm 2.0 \pm 0.5$	5
			≥ 1500	NB3i, LT12, HT4i	0.13 ± 0.01	< 0.01	$2.9 \pm 0.9 \pm 0.3$	3
		[450, 600]	[500, 1000]	NB3i, LT3, HT01	0.03 ± 0.01	0.29 ± 0.07	$1.4 \pm 0.5 \pm 0.2$	2
			[1000, 1500]	NB3i, LT3, HT23	0.09 ± 0.01	0.20 ± 0.06	$0.72 \pm 0.38 \pm 0.07$	1
			≥ 1500	NB3i, LT3, HT4i	0.20 ± 0.02	< 0.01	$0.66 \pm 0.44 \pm 0.07$	0
		≥ 600	≥ 500	NB3i, LT4i, HT0i	1.85 ± 0.05	0.23 ± 0.06	$1.7 \pm 0.7 \pm 0.2$	2
≥ 9	$= 1$	[250, 450]	[500, 1500]	NB1, LT12, HT03	0.01 ± 0.01	0.90 ± 0.12	$7.9 \pm 0.9 \pm 0.7$	7
			≥ 1500	NB1, LT12, HT4i	0.03 ± 0.01	0.02 ± 0.02	$2.2 \pm 0.7 \pm 0.2$	1
		≥ 450	[500, 1500]	NB1, LT3i, HT03	0.13 ± 0.01	0.72 ± 0.11	$1.1 \pm 0.4 \pm 0.2$	0
			≥ 1500	NB1, LT3i, HT4i	0.38 ± 0.02	0.10 ± 0.04	$0.50 \pm 0.26 \pm 0.06$	1
	$= 2$	[250, 450]	[500, 1500]	NB2, LT12, HT03	0.02 ± 0.01	1.15 ± 0.14	$7.3 \pm 0.8 \pm 0.5$	9
			≥ 1500	NB2, LT12, HT4i	0.08 ± 0.01	< 0.01	$2.8 \pm 0.8 \pm 0.3$	4
		≥ 450	[500, 1500]	NB2, LT3i, HT03	0.23 ± 0.02	0.83 ± 0.12	$0.71 \pm 0.24 \pm 0.09$	2
			≥ 1500	NB2, LT3i, HT4i	0.72 ± 0.03	0.20 ± 0.05	$0.59 \pm 0.30 \pm 0.07$	1
	≥ 3	[250, 450]	[500, 1500]	NB3i, LT12, HT03	0.03 ± 0.01	0.79 ± 0.11	$3.6 \pm 0.6 \pm 0.3$	3
			≥ 1500	NB3i, LT12, HT4i	0.13 ± 0.01	< 0.01	$0.83 \pm 0.34 \pm 0.07$	0
		≥ 450	[500, 1500]	NB3i, LT3i, HT03	0.31 ± 0.02	0.26 ± 0.06	$0.33 \pm 0.16 \pm 0.07$	0
			≥ 1500	NB3i, LT3i, HT4i	1.04 ± 0.04	0.17 ± 0.05	$0.05 \pm 0.05 \pm 0.01$	0

Table 7: Results table of the 0-tag regions, 36fb^{-1}

n_{jet}	L_{T} [GeV]	H_{T} [GeV]	Bin name	Signal T5qqqqWW $m_{\tilde{g}}/m_{\tilde{\chi}^0}$ [TeV] (1.5/1.0)	(1.9/0.1)	Predicted background	Observed
5	[250, 350]	[500, 750]	LT0, HT0	1.82 ± 0.29	< 0.01	101.91 ± 47.55	111
		≥ 750	LT0, HT1i	0.21 ± 0.09	0.01 ± 0.01	76.73 ± 16.19	100
	[350, 450]	[500, 750]	LT1, HT0	2.25 ± 0.32	< 0.01	24.43 ± 14.78	25
		≥ 750	LT1, HT1i	0.29 ± 0.11	0.04 ± 0.01	22.78 ± 8.29	22
	[450, 650]	[500, 750]	LT2, HT0	3.02 ± 0.37	< 0.01	14.46 ± 6.5	17
		[750, 1250]	LT2, HT12	1.4 ± 0.25	0.04 ± 0.02	12.13 ± 4.68	10
		≥ 1250	LT2, HT3i	0.08 ± 0.06	0.25 ± 0.04	4.15 ± 1.72	2
	≥ 650	[500, 750]	LT3i, HT0	0.74 ± 0.18	0.01 ± 0.01	2.32 ± 1.49	5
		[750, 1250]	LT3i, HT12	0.49 ± 0.15	0.12 ± 0.03	5.79 ± 1.96	6
		≥ 1250	LT3i, HT3i	0.14 ± 0.07	1.15 ± 0.08	2.74 ± 1.26	0
[6, 7]	[250, 350]	[500, 1000]	LT0, HT01	3.02 ± 0.36	< 0.01	89.32 ± 38.21	85
		≥ 1000	LT0, HT2i	0.31 ± 0.1	0.09 ± 0.02	30.94 ± 5.08	33
	[350, 450]	[500, 1000]	LT1, HT01	4.13 ± 0.41	0.01 ± 0.01	18.91 ± 10.89	31
		≥ 1000	LT1, HT2i	0.52 ± 0.14	0.14 ± 0.03	9.51 ± 2.34	8
	[450, 650]	[500, 750]	LT2, HT0	3.63 ± 0.39	< 0.01	5.71 ± 3.31	13
		[750, 1250]	LT2, HT12	3.79 ± 0.39	0.03 ± 0.01	8.21 ± 3.15	8
		≥ 1250	LT2, HT3i	0.36 ± 0.12	0.47 ± 0.05	3.61 ± 1.78	4
	≥ 650	[500, 750]	LT3i, HT0	0.89 ± 0.19	< 0.01	0.79 ± 0.53	3
		[750, 1250]	LT3i, HT12	1.77 ± 0.26	0.15 ± 0.03	3.63 ± 1.37	5
		≥ 1250	LT3i, HT3i	0.83 ± 0.18	2.83 ± 0.12	1.83 ± 0.86	1
≥ 8	[250, 350]	[500, 1000]	LT0, HT01	0.88 ± 0.18	< 0.01	6.96 ± 2.83	16
		≥ 1000	LT0, HT2i	0.26 ± 0.09	0.03 ± 0.01	6.32 ± 1.17	4
	[350, 450]	[500, 1000]	LT1, HT01	0.55 ± 0.14	< 0.01	1.67 ± 0.77	3
		≥ 1000	LT1, HT2i	0.72 ± 0.15	0.11 ± 0.02	2.65 ± 0.89	4
	[450, 650]	[500, 1250]	LT2, HT02	2.07 ± 0.26	0.01 ± 0.01	0.63 ± 0.32	0
		≥ 1250	LT2, HT3i	0.45 ± 0.12	0.3 ± 0.04	0.68 ± 0.35	1
	≥ 650	[500, 1250]	LT3i, HT02	0.97 ± 0.18	0.04 ± 0.01	0.27 ± 0.23	1
		≥ 1250	LT3i, HT3i	1.12 ± 0.18	1.37 ± 0.08	0.38 ± 0.24	1

References

[1] P. Ramond, "Dual theory for free fermions", *Phys. Rev. D* **3** (1971) 2415, doi:10.1103/PhysRevD.3.2415.

[2] Y. A. Golfand and E. P. Likhtman, "Extension of the algebra of Poincaré group generators and violation of P invariance", *JETP Lett.* **13** (1971) 323.

[3] A. Neveu and J. H. Schwarz, "Factorizable dual model of pions", *Nucl. Phys. B* **31** (1971) 86, doi:10.1016/0550-3213(71)90448-2.

[4] D. V. Volkov and V. P. Akulov, "Possible universal neutrino interaction", *JETP Lett.* **16** (1972) 438.

[5] J. Wess and B. Zumino, "A Lagrangian model invariant under supergauge transformations", *Phys. Lett. B* **49** (1974) 52, doi:10.1016/0370-2693(74)90578-4.

[6] J. Wess and B. Zumino, "Supergauge transformations in four dimensions", *Nucl. Phys. B* **70** (1974) 39, doi:10.1016/0550-3213(74)90355-1.

[7] P. Fayet, "Supergauge invariant extension of the Higgs mechanism and a model for the electron and its neutrino", *Nucl. Phys. B* **90** (1975) 104, doi:10.1016/0550-3213(75)90636-7.

[8] H. P. Nilles, "Supersymmetry, supergravity and particle physics", *Phys. Rep.* **110** (1984) 1, doi:10.1016/0370-1573(84)90008-5.

[9] G. R. Farrar and P. Fayet, "Phenomenology of the production, decay, and detection of new hadronic states associated with supersymmetry", *Phys. Lett. B* **76** (1978) 575, doi:10.1016/0370-2693(78)90858-4.

[10] CMS Collaboration, "Search for supersymmetry in events with one lepton and multiple jets in proton-proton collisions at sqrt(s) = 13 TeV ", *PRD* **???** (2016) ???, doi:???, arXiv:1609.09386.

[11] CMS Collaboration, "Search for supersymmetry in pp collisions at $\sqrt{s} = 7$ TeV in events with a single lepton, jets, and missing transverse momentum", *Eur. Phys. J. C* **73** (2013) 2404, doi:10.1140/epjc/s10052-013-2404-z, arXiv:1212.6428.

[12] CMS Collaboration, "Search for supersymmetry in final states with a single lepton, b-quark jets, and missing transverse energy in proton-proton collisions at $\sqrt{s} = 7$ TeV", *Phys. Rev. D* **87** (2013) 052006, doi:10.1103/PhysRevD.87.052006, arXiv:1211.3143.

[13] ATLAS Collaboration, "Further search for supersymmetry at $\sqrt{s} = 7$ TeV in final states with jets, missing transverse momentum and isolated leptons with the ATLAS detector", *Phys. Rev. D* **86** (2012) 092002, doi:10.1103/PhysRevD.86.092002, arXiv:1208.4688.

[14] CMS Collaboration, "Search for supersymmetry in pp collisions at $\sqrt{s} = 8$ TeV in events with a single lepton, large jet multiplicity, and multiple b jets", *Phys. Lett. B* **733** (2014) 328, doi:10.1016/j.physletb.2014.04.023, arXiv:1311.4937.

[15] ATLAS Collaboration, "Search for squarks and gluinos in events with isolated leptons, jets and missing transverse momentum at $\sqrt{s} = 8$ TeV with the ATLAS detector", *JHEP* **04** (2015) 116, doi:10.1007/JHEP04(2015)116, arXiv:1501.03555.

[16] ATLAS Collaboration, "Search for strong production of supersymmetric particles in final states with missing transverse momentum and at least three b-jets at $\sqrt{s} = 8$ TeV proton-proton collisions with the ATLAS detector", *JHEP* **10** (2014) 024, doi:10.1007/JHEP10(2014)024, arXiv:1407.0600.

[17] CMS Collaboration, "Search for supersymmetry in pp collisions at $\sqrt{s} = 13$ TeV in the single-lepton final state using the sum of masses of large-radius jets", *JHEP* **08** (2016) 122, doi:10.1007/JHEP08(2016)122, arXiv:1605.04608.

[18] ATLAS Collaboration, "Search for gluinos in events with an isolated lepton, jets and missing transverse momentum at $\sqrt{s}$ = 13 TeV with the ATLAS detector", (2016). arXiv:1605.04285. Submitted to *EPJC*.

[19] ATLAS Collaboration, "Search for pair production of gluinos decaying via stop and sbottom in events with *b*-jets and large missing transverse momentum in pp collisions at $\sqrt{s} = 13$ TeV with the ATLAS detector", (2016). arXiv:1605.09318.

[20] N. Arkani-Hamed et al., "MARMOSET: The path from LHC data to the new standard model via on-shell effective theories", (2007). arXiv:hep-ph/0703088.

[21] J. Alwall, P. C. Schuster, and N. Toro, "Simplified models for a first characterization of new physics at the LHC", *Phys. Rev. D* **79** (2009) 075020, doi:10.1103/PhysRevD.79.075020, arXiv:0810.3921.

[22] J. Alwall, M.-P. Le, M. Lisanti, and J. G. Wacker, "Model-independent jets plus missing energy searches", *Phys. Rev. D* **79** (2009) 015005, doi:10.1103/PhysRevD.79.015005, arXiv:0809.3264.

[23] D. Alves et al., "Simplified models for LHC new physics searches", *J. Phys. G* **39** (2012) 105005, doi:10.1088/0954-3899/39/10/105005, arXiv:1105.2838.

[24] CMS Collaboration, "The CMS experiment at the CERN LHC", *JINST* **3** (2008) S08004, doi:10.1088/1748-0221/3/08/S08004.

[25] CMS Collaboration, "Particle-flow event reconstruction in CMS and performance for jets, taus, and $E_{\mathrm{T}}^{\mathrm{miss}}$", CMS Physics Analysis Summary CMS-PAS-PFT-09-001, CERN, 2009.

[26] CMS Collaboration, "Commissioning of the particle-flow event with the first LHC collisions recorded in the CMS detector", CMS Physics Analysis Summary CMS-PAS-PFT-10-001, CERN, 2010.

[27] CMS Collaboration, "Performance of electron reconstruction and selection with the CMS detector in proton-proton collisions at $\sqrt{s} = 8$ TeV", *JINST* **10** (2015) P06005, doi:10.1088/1748-0221/10/06/P06005, arXiv:1502.02701.

[28] CMS Collaboration, "Performance of CMS muon reconstruction in pp collision events at $\sqrt{s} = 7$ TeV", *JINST* **7** (2012) P10002, doi:10.1088/1748-0221/7/10/P10002, arXiv:1206.4071.

[29] M. Cacciari, G. P. Salam, and G. Soyez, "The Anti-k(t) jet clustering algorithm", *JHEP* **04** (2008) 063, doi:10.1088/1126-6708/2008/04/063, arXiv:0802.1189.

[30] CMS Collaboration, "Determination of jet energy calibration and transverse momentum resolution in CMS", *JINST* **6** (2011) P11002, doi:10.1088/1748-0221/6/11/P11002, arXiv:1107.4277.

[31] M. Cacciari, G. P. Salam, and G. Soyez, "FastJet User Manual", *Eur. Phys. J.* **C72** (2012) 1896, doi:10.1140/epjc/s10052-012-1896-2, arXiv:1111.6097.

[32] M. Cacciari and G. P. Salam, "Pileup subtraction using jet areas", *Phys. Lett. B* **659** (2008) 119, doi:10.1016/j.physletb.2007.09.077, arXiv:0707.1378.

[33] CMS Collaboration, "Jet energy scale and resolution in the CMS experiment in pp collisions at 8 TeV", *JINST* **12** (2017) P02014, doi:10.1088/1748-0221/12/02/P02014, arXiv:1607.03663.

[34] CMS Collaboration, "Identification of b-quark jets with the CMS experiment", *JINST* **8** (2013) P04013, doi:10.1088/1748-0221/8/04/P04013, arXiv:1211.4462.

[35] CMS Collaboration, "Identification of b quark jets at the CMS Experiment in the LHC Run 2", CMS Physics Analysis Summary CMS-PAS-BTV-15-001, CERN, 2016.

[36] CMS Collaboration, "Performance of b tagging at $\sqrt{s} = 8$ TeV in multijet, $\mathrm{t\bar{t}}$ and boosted topology events", CMS Physics Analysis Summary CMS-PAS-BTV-13-001, CERN, 2013.

[37] J. Alwall et al., "MadGraph5: going beyond", *JHEP* **06** (2011) 128, doi:10.1007/JHEP06(2011)128, arXiv:1106.0522.

[38] NNPDF Collaboration, "Parton distributions for the LHC Run II", *JHEP* **04** (2015) 040, doi:10.1007/JHEP04(2015)040, arXiv:1410.8849.

[39] P. Nason, "A new method for combining NLO QCD with shower Monte Carlo algorithms", *JHEP* **11** (2004) 040, doi:10.1088/1126-6708/2004/11/040, arXiv:hep-ph/0409146.

[40] S. Frixione, P. Nason, and C. Oleari, "Matching NLO QCD computations with parton shower simulations: the POWHEG method", *JHEP* **11** (2007) 070, doi:10.1088/1126-6708/2007/11/070, arXiv:0709.2092.

[41] S. Alioli, P. Nason, C. Oleari, and E. Re, "A general framework for implementing NLO calculations in shower Monte Carlo programs: the POWHEG BOX", *JHEP* **06** (2010) 043, doi:10.1007/JHEP06(2010)043, arXiv:1002.2581.

[42] S. Alioli, P. Nason, C. Oleari, and E. Re, "NLO single-top production matched with shower in POWHEG: s- and t-channel contributions", *JHEP* **09** (2009) 111, doi:10.1088/1126-6708/2009/09/111, arXiv:0907.4076. [Erratum: doi:10.1007/JHEP02(2010)011].

[43] E. Re, "Single-top Wt-channel production matched with parton showers using the POWHEG method", *Eur. Phys. J. C* **71** (2011) 1547, doi:10.1140/epjc/s10052-011-1547-z, arXiv:1009.2450.

[44] J. Alwall et al., "The automated computation of tree-level and next-to-leading order differential cross sections, and their matching to parton shower simulations", *JHEP* **07** (2014) 079, doi:10.1007/JHEP07(2014)079, arXiv:1405.0301.

[45] T. Melia, P. Nason, R. Rontsch, and G. Zanderighi, "$\mathrm{W^+W^-}$, WZ and ZZ production in the POWHEG BOX", *JHEP* **11** (2011) 078, doi:10.1007/JHEP11(2011)078, arXiv:1107.5051.

[46] M. Beneke, P. Falgari, S. Klein, and C. Schwinn, "Hadronic top-quark pair production with NNLL threshold resummation", *Nucl. Phys. B* **855** (2012) 695, doi:10.1016/j.nuclphysb.2011.10.021, arXiv:1109.1536.

[47] M. Cacciari et al., "Top-pair production at hadron colliders with next-to-next-to-leading logarithmic soft-gluon resummation", *Phys. Lett. B* **710** (2012) 612, doi:10.1016/j.physletb.2012.03.013, arXiv:1111.5869.

[48] P. Bärnreuther, M. Czakon, and A. Mitov, "Percent Level Precision Physics at the Tevatron: First Genuine NNLO QCD Corrections to $q\bar{q} \to t\bar{t} + X$", *Phys. Rev. Lett.* **109** (2012) 132001, doi:10.1103/PhysRevLett.109.132001, arXiv:1204.5201.

[49] M. Czakon and A. Mitov, "NNLO corrections to top-pair production at hadron colliders: the all-fermionic scattering channels", *JHEP* **12** (2012) 054, doi:10.1007/JHEP12(2012)054, arXiv:1207.0236.

[50] M. Czakon and A. Mitov, "NNLO corrections to top pair production at hadron colliders: the quark-gluon reaction", *JHEP* **01** (2013) 080, doi:10.1007/JHEP01(2013)080, arXiv:1210.6832.

[51] M. Czakon, P. Fiedler, and A. Mitov, "Total Top-Quark Pair-Production Cross Section at Hadron Colliders Through $O(\alpha_S^4)$", *Phys. Rev. Lett.* **110** (2013) 252004, doi:10.1103/PhysRevLett.110.252004, arXiv:1303.6254.

[52] R. Gavin, Y. Li, F. Petriello, and S. Quackenbush, "W Physics at the LHC with FEWZ 2.1", *Comput. Phys. Commun.* **184** (2013) 208, doi:10.1016/j.cpc.2012.09.005, arXiv:1201.5896.

[53] R. Gavin, Y. Li, F. Petriello, and S. Quackenbush, "FEWZ 2.0: A code for hadronic Z production at next-to-next-to-leading order", *Comput. Phys. Commun.* **182** (2011) 2388, doi:10.1016/j.cpc.2011.06.008, arXiv:1011.3540.

[54] T. Sjöstrand et al., "An Introduction to PYTHIA 8.2", *Comput. Phys. Commun.* **191** (2015) 159, doi:10.1016/j.cpc.2015.01.024, arXiv:1410.3012.

[55] W. Beenakker, R. Höpker, M. Spira, and P. M. Zerwas, "Squark and gluino production at hadron colliders", *Nucl. Phys. B* **492** (1997) 51, doi:10.1016/S0550-3213(97)00084-9, arXiv:hep-ph/9610490.

[56] A. Kulesza and L. Motyka, "Threshold resummation for squark-antisquark and gluino-pair production at the LHC", *Phys. Rev. Lett.* **102** (2009) 111802, doi:10.1103/PhysRevLett.102.111802, arXiv:0807.2405.

[57] A. Kulesza and L. Motyka, "Soft gluon resummation for the production of gluino-gluino and squark-antisquark pairs at the LHC", *Phys. Rev. D* **80** (2009) 095004, doi:10.1103/PhysRevD.80.095004, arXiv:0905.4749.

[58] W. Beenakker et al., "Soft-gluon resummation for squark and gluino hadroproduction", *JHEP* **12** (2009) 041, doi:10.1088/1126-6708/2009/12/041, arXiv:0909.4418.

[59] W. Beenakker et al., "Squark and gluino hadroproduction", *Int. J. Mod. Phys. A* **26** (2011) 2637, doi:10.1142/S0217751X11053560, arXiv:1105.1110.

[60] S. Agostinelli et al., "GEANT4 — a simulation toolkit", *Nucl. Instr. and Meth. A* **506** (2003) 250, doi:10.1016/S0168-9002(03)01368-8.

[61] CMS CollaborationS. Abdullin, et al., "The Fast Simulation of the CMS Detector at LHC", in *Int'l Conf. on Computing in High Energy and Nuclear Physics (CHEP 2010)*. 2011. Journal of Physics: Conference Series, 331 (2011), 032049. doi:10.1088/1742-6596/331/3/032049.

[62] C. Lester and D. Summers, "Measuring masses of semi-invisibly decaying particle pairs pr oduced at hadron colliders", *Phys. Lett. B* **463** (1999) 5, doi:10.1016/S0370-2693(99)00945-4.

[63] ATLAS Collaboration, "Measurement of the Inelastic Proton-Proton Cross Section at $\sqrt{s} = 13$ TeV with the ATLAS Detector at the LHC", (2016). arXiv:1606.02625. Submitted to *PRL*.

[64] CMS Collaboration, "Measurement of the production cross section of the W boson in association with two b jets in pp collisions at $\sqrt{s}$ = 8 TeV", arXiv:1608.07561. Submitted to *EPJC*.

[65] Z. Bern et al., "Left-handed W bosons at the LHC", *Phys. Rev. D* **84** (2011) 034008, doi:10.1103/PhysRevD.84.034008, arXiv:1103.5445.

[66] CMS Collaboration, "Angular coefficients of Z bosons produced in pp collisions at $\sqrt{s} = 8$ TeV and decaying to $\mu^+\mu^-$ as a function of transverse momentum and rapidity", *Phys. Lett. B* **750** (2015) 154, doi:10.1016/j.physletb.2015.08.061, arXiv:1504.03512.

[67] CMS Collaboration, "Measurement of the Polarization of W Bosons with Large Transverse Momenta in W+Jets Events at the LHC", *Phys. Rev. Lett.* **107** (2011) 021802, doi:10.1103/PhysRevLett.107.021802, arXiv:1104.3829.

[68] ATLAS Collaboration, "Measurement of the polarisation of W bosons produced with large transverse momentum in pp collisions at $\sqrt{s} = 7$ TeV with the ATLAS experiment", *Eur. Phys. J. C* **72** (2012) 2001, doi:10.1140/epjc/s10052-012-2001-6, arXiv:1203.2165.

[69] CMS Collaboration, "CMS Luminosity Measurement for the 2015 Data Taking Period", CMS Physics Analysis Summary CMS-PAS-LUM-15-001, CERN, 2016.

[70] G. Cowan, K. Cranmer, E. Gross, and O. Vitells, "Asymptotic formulae for likelihood-based tests of new physics", *Eur. Phys. J. C* **71** (2011) 1554, doi:10.1140/epjc/s10052-011-1554-0, arXiv:1007.1727. [Erratum: doi:10.1140/epjc/s10052-013-2501-z].

[71] T. Junk, "Confidence level computation for combining searches with small statistics", *Nucl. Instr. and Meth. A* **434** (1999) 435, doi:10.1016/S0168-9002(99)00498-2, arXiv:hep-ex/9902006.

[72] A. L. Read, "Presentation of search results: the CL_s technique", *J. Phys. G* **28** (2002) 2693, doi:10.1088/0954-3899/28/10/313.